

1
2
3
4
5
6
7
8
9
10
11
12
13
14
15
16
17
18
19
20

Detecting Clouds Associated with Jet Engine Ice Crystal Icing

Julie Haggerty, Eric Defer, Adrianus de Laat, Kristopher Bedka, Jean-Marc Moisselin,
Rodney Potts, Julien Delanoë, Frédéric Parol, Alice Grandin, and Stephanie DiVito

For Submission to the Bulletin of the American Meteorological Society (InBox Article)

28 April 2018

AFFILIATIONS: Haggerty, National Center for Atmospheric Research, Boulder, Colorado; Defer, Laboratoire d'Aérodynamique, Université de Toulouse, CNRS, OMP, UPS, Toulouse, France; de Laat, KNMI, de Bilt, the Netherlands; Bedka, NASA Langley Research Center, Hampton, Virginia; Moisselin, Météo-France, Toulouse, France; Potts, Bureau of Meteorology, Melbourne, Australia; Delanoë, LATMOS, IPSL, UVSQ, Guyancourt, France; Parol, LOA, Université de Lille – Sciences et Technologies, CNRS, Lille, France; Grandin, AIRBUS S.A.S., Toulouse, France; DiVito, FAA Wm. J. Hughes Technical Center, Atlantic City, New Jersey

Corresponding Author: Julie Haggerty, haggerty@ucar.edu

21

Abstract

22

23

24

25

26

27

28

29

In the past two decades over 150 jet engine power-loss and damage events have been attributed to a phenomenon known as Ice Crystal Icing (ICI). Ingestion of large numbers of ice particles into the engine core are thought to be responsible for these events which typically occur at high altitudes near large convective systems in tropical air masses. In recent years scientists, engineers, aviation regulators and airlines from around the world have collaborated to better understand the relevant meteorological processes associated with ICI events, solve critical engineering problems, develop new certification standards, and devise mitigation strategies for the aviation industry.

30

31

32

33

34

35

36

One area of research is the development of nowcasting techniques based on available remote sensing technology and Numerical Weather Prediction (NWP) models to identify areas of high ice water content (IWC) and enable the provision of alerts to the aviation industry. Multiple techniques have been developed using geostationary and polar orbiting satellite products, numerical weather prediction (NWP) model fields, and ground based radar data as the basis for HIWC products. Targeted field experiments in tropical regions with high incidence of ICI events have provided data for product validation and refinement of these methods.

37

38

39

40

Beginning in 2015, research teams have assembled at a series of annual workshops to exchange ideas and standardize methods for evaluating performance of HIWC detection products. This paper provides an overview of the approaches used and the current skill for identifying HIWC conditions. Recommendations for future work in this area are also presented.

41 Ingestion of large amounts of ice crystals by jet engines, known as the Ice Crystal Icing (ICI)
42 hazard, appears to be the culprit in over 150 jet engine power-loss and damage events during
43 the past two decades (Fig. 1). Typically occurring near tropical convective systems, heated inlets
44 used by an aircraft's Air Data System also appear to be vulnerable to high ice water content
45 (IWC) conditions. Although the heat within an engine or inlet would presumably prevent any ice
46 build-up, analyses of engine power-loss events attributed to ICI together with wind tunnel
47 testing suggest that significant amounts of ice can accrete inside sensitive parts of an aircraft
48 engine. Ice accretion and subsequent ice shedding into engine cores during flight can adversely
49 affect engine performance and damage engine components. Early research by Lawson et al.
50 (1998) and Mason et al. (2006) suggested that engine power-loss events were attributable to
51 ingestion of high concentrations of small ice crystals. The occurrence of engine power-loss
52 under atmospheric conditions not formerly recognized as hazardous initiated investigation of
53 the clouds, convection, and microphysics associated with ICI events. Analyses of the
54 meteorological conditions associated with these events revealed several common attributes. ICI
55 hazards tend to occur near cores of deep convection and associated cirrus anvils. Flight level
56 radar reflectivity is generally below 20-30 dBZ (Grzych and Mason, 2010), suggesting that small
57 ice crystals constitute the bulk of the ice mass encountered. Areas of heavy precipitation below
58 flight level are sometimes observed. Any reports of turbulence are generally light to moderate,
59 and there is no significant airframe ice accretion, precluding the existence of supercooled liquid
60 water. ICI events occur over a temperature range of -58°C to -3°C and at altitudes from 11000 –
61 45000 ft. according to Bravin et al. (2015).

62 Following analysis of ICI events, an international consortium of researchers assembled to
63 investigate the scientific and engineering aspects of ice crystal icing. The USA-led High Ice
64 Water Content (HIWC) and the European High Altitude Ice Crystal (HAIC) projects brought
65 researchers together with aviation engineers, operators and regulators from Europe, North
66 America, and Australia. Their objectives are to develop a better understanding of the relevant
67 meteorology, explore critical engineering questions, develop new aircraft certification
68 standards, and formulate mitigation strategies for the aviation industry. Sponsored by the U.S.
69 Federal Aviation Administration (FAA), the European Union 7th Framework Programme for
70 Research and Technological Development (FP7), NASA, the European Aviation Safety Agency
71 (EASA), the Australian Bureau of Meteorology (BOM), Transport Canada, Airbus, and Boeing,
72 multiple research teams are investigating the meteorological processes associated with high
73 IWC.

74 A central objective of these efforts is to understand the dynamic, thermodynamic, and
75 microphysical cloud processes that result in potentially hazardous concentrations of ice crystals
76 in some convective clouds. A review of current research in these areas is beyond the scope of
77 this paper, but can be found elsewhere (e.g., Leroy et al. (2017), Ackerman et al. (2015),
78 Stanford et al. (2017)).

79 **DETECTION OF HIGH IWC CONDITIONS**

80 An area of active research within the international consortium is the development of high
81 IWC satellite detection and nowcasting techniques based on available remote sensing
82 technology and numerical weather prediction (NWP) models. These techniques attempt to
83 identify areas of high IWC and could enable the provision of alerts to the aviation industry. Such

84 information is needed because, while new engine certification standards may largely mitigate
85 the risks associated with ICI for future aircraft engines, there is a large, currently susceptible
86 fleet which will be operating for many years. Thus there is a recognized need for nowcasting
87 guidance products to support flight planning and management of the strategic and tactical
88 response for these aircraft.

89 Various research teams are investigating methods for detecting the high IWC conditions
90 associated with ICI. Multiple techniques have been developed using geostationary and polar
91 orbiting satellite products, NWP model fields, and ground based radar data as the basis for high
92 IWC warning products (Table 1). Described below are the approaches of teams within the
93 original HIWC-HAIC research partnership.

94 *MSG-CPP High IWC Mask*

95 The Royal Netherlands Meteorological Institute (KNMI) developed a geostationary satellite
96 data product for identifying atmospheric conditions thought to favor ICI. Using daytime
97 retrievals of cloud top height, cloud top temperature, and condensed water path from the
98 Cloud Physical Properties (CPP) algorithm, the method sets thresholds on each variable to
99 assemble a mask indicating areas of high IWC. The mask was successfully implemented on near-
100 real-time imagery from various geostationary satellites. It has been evaluated against
101 measurements from several field campaigns, has been used for real-time field campaign
102 planning purposes, and applied to construct climatologies of the occurrence of ICI conditions.
103 The MSG-CPP High IWC Mask is currently available via the KNMI MSG-CPP webportal
104 (<http://msgcpp.knmi.nl>). The algorithm was also adapted to low orbit MODIS observations and
105 has been integrated in the Rapidly Developing Thunderstorms (RDT) data product (see below).

106 *DARDAR products*

107 The DARDAR (raDAR/liDAR) product provides cloud properties by combining, through a
108 synergistic variational algorithm, coincident spaceborne measurements of both CloudSat (95
109 GHz) radar and the CALIPSO (532 and 1064 nm) lidar, both instruments being part of the low
110 orbit A-Train mission. The DARDAR algorithm retrieves vertical profiles of IWC, effective radius,
111 particle size distribution, cloud phase and cloud classification. It utilizes lidar sensitivity to highly
112 concentrated small ice crystals along with the capability of the radar to penetrate optically thick
113 ice clouds. The DARDAR product was used to statistically and geographically document at the
114 global scale the occurrence of high IWC, whatever its vertical altitude, and also to tune and
115 validate other high IWC products. A similar algorithm, based on radar alone, was applied to the
116 RAdar SysTem Airborne (RASTA) cloud radar observations collected during various field
117 campaigns, providing closure between airborne *in situ* measurements and remote sensing
118 retrievals.

119 *NASA Langley Research Center (LaRC) Probability of HIWC (PHIWC)*

120 Airborne in-situ IWC observations collected during three field campaigns (described below)
121 were used to identify GOES and MTSAT-1R satellite-derived parameters coincident with high
122 IWC. Analysis of these flights show 1) an exponential IWC increase during flight within 40 km of
123 a convective updraft region, 2) an exponential IWC increase during flight within or beneath
124 increasingly cold cloud tops, normalized by the regional Numerical Weather Prediction (NWP)
125 model tropopause temperature (Fig. 2a), and 3) a linear IWC increase with increasing cloud
126 optical depth (daytime only) derived using the LaRC Satellite CLOud and Radiative Property
127 retrieval System (SatCORPS). These relationships were used to derive fuzzy logic membership

128 functions that serve as the foundation for the NASA LaRC Probability of High IWC (PHIWC)
129 product (Fig 2c). Automated pattern recognition of overshooting cloud tops and anvil texture
130 are used to define convective updraft regions (Fig 2b). The PHIWC product is designed to
131 operate during both day and night, and can be generated using any global polar-orbiting or
132 geostationary visible/IR imager.

133 *Algorithm for the Prediction of HIWC Areas (ALPHA)*

134 ALPHA, developed at the National Center for Atmospheric Research (NCAR), is a 3-
135 dimensional diagnostic tool that uses operationally available satellite data, NWP model data,
136 and ground based radar data (where available) as input. The 3-dimensional NWP model and
137 radar data are blended with the 2-dimensional satellite data via a set of fuzzy logic membership
138 functions that exploit the strengths of each data set. A machine learning technique is applied to
139 tune the algorithm using research aircraft measurements in high IWC conditions. A technique
140 known as Particle Swarm Optimization is used to select specific input variables, define
141 membership functions, and determine weighting factors for optimal blending of the various
142 data. Output from ALPHA is a 3-dimensional gridded field of HIWC Potential (which can be
143 thought of as an uncalibrated probability). The HIWC Potential field consists of output based on
144 satellite, model, and radar data (3-input algorithm), and on satellite and model data only where
145 radar data are not available (2-input algorithm). An example of HIWC Potential, which blends
146 output from the 2- and 3-input versions of the algorithm, is shown in Fig. 3 with *in situ* IWC
147 measurements superimposed.

148 *Rapidly Developing Thunderstorms (RDT)*

149 RDT (Rapidly Developing Thunderstorm) software is developed by Météo-France in the
150 framework of Eumetsat’s Satellite Application Facility for Nowcasting (NWCSAF). RDT uses
151 brightness temperatures from geostationary satellites with the option of using NWP (Numerical
152 Weather Prediction) products or lightning data. RDT detects, tracks and extrapolates
153 thunderstorms cells. RDT also characterizes observed systems with different attributes such as
154 cooling rate, top of thunderstorm, horizontal extension, etc. High IWC values are often
155 associated with deep convection and especially strong updrafts that inject significant quantities
156 of water into the upper troposphere.

157 **FIELD EXPERIMENTS**

158 A series of field experiments in tropical regions with high incidence of ICI events provided
159 research aircraft data for development and validation of nowcasting methods (Strapp et al.,
160 2016; Dezitter et al., 2013). The HIWC and HAIC projects jointly conducted experiments in
161 Darwin, Australia (23 flights by the SAFIRE Falcon 20 in Jan-Mar 2014; Fig. 4) and Cayenne,
162 French Guiana (17 flights by the SAFIRE Falcon 20 and 10 flights by the Canadian Convair 580
163 during May 2015). A NASA-led HIWC team executed the HIWC Radar Study in Ft. Lauderdale, FL
164 (10 flights by the NASA D-8 in Aug 2015). The HAIC project conducted a subsequent experiment
165 with the Airbus A340 MSN1 flight test aircraft in Darwin and Reunion Island in January 2016.

166 The payload for all experiments included cloud microphysics probes, total water content
167 (TWC) sensors, and cloud radar. Of particular interest for nowcast product development are
168 measurements of TWC from a newly developed isokinetic evaporator known as the Isokinetic
169 Probe (IKP2) (Davison et al., 2016) and an existing hot wire probe (ROBUST probe), as well as
170 vertical IWC profiles from the airborne RASTA cloud radar.

171 **COLLABORATIVE RESEARCH**

172 Beginning in 2015, the HAIC and HIWC nowcasting research teams have assembled at a
173 series of dedicated workshops to foster international collaboration on development of high IWC
174 diagnosis and forecasting methods. Meeting objectives have focused on sharing progress
175 toward development of global HIWC products and standardizing techniques for evaluating
176 performance of the products. Table 2 lists meeting dates and locations. Meeting agendas
177 featured presentations by each group describing methods used for high IWC detection,
178 subsequent discussions of the various approaches, and sharing of analyses by each group of
179 designated case studies from the field experiments.

180 **PRODUCT PERFORMANCE**

181 One outcome of these workshops is recognition that validation of high IWC products is
182 complex. The work done by the various HIWC-HAIC teams demonstrates that assessing
183 performance of these products and comparing them in a meaningful way is not
184 straightforward. The challenges arise from differences in product attributes as well as validation
185 approaches. Performance statistics are affected by various issues such as:

- 186 1) Sensitivity of results to assumptions used, e.g., the IWC threshold used to define high
187 IWC.
- 188 2) Use of differing criteria to co-locate *in situ* data with satellite/model/radar data and to
189 account for spatio-temporal differences in the data sets.
- 190 3) Differing objectives of products, e.g, RDT identifies convective systems; the MSG-CPP
191 High IWC Mask provides a binary (yes/no) indicator based on the maximum IWC in a
192 vertical column; PHIWC and ALPHA estimate the potential for high IWC.

193 The HIWC-HAIC teams have worked toward consistent evaluation methods where possible
194 (e.g., issues (1) and (2) noted above), but inherent differences in the various approaches
195 continue to complicate comparison of product performance. Nevertheless, it is still important
196 for the community to gain a basic understanding of the accuracy of existing products, so each
197 team has compiled relevant statistics to evaluate its approach.

198 The MSG-CPP High IWC Mask product gives a typical probability of detection (POD) around
199 60-80% of clouds in which DARDAR IWC exceeds 1 g/m^3 , with a similar false alarm ratio when
200 compared with DARDAR IWC measurements (Fig. 5). The MSG-CPP High IWC mask also rejects
201 the large majority of DARDAR IWC profiles where the maximum IWC does not exceed this IWC
202 threshold value. The LaRC PHIWC and ALPHA HIWC Potential products attempt to pinpoint
203 where within deep convection high IWC conditions *are likely*, a differing goal relative to the
204 MSG-CPP product which masks areas where high IWC *is possible* throughout the cloud vertical
205 depth. Both PHIWC and ALPHA have been verified against airborne TWC measurements from
206 the IKP2. The two-dimensional PHIWC product gives a POD ranging from 60-80% and a false
207 alarm rate of 20-35%, with best performance offered during daylight hours when cloud optical
208 depth and visible texture retrievals are available and for extremely high IWC values (e.g. > 2.0
209 gm^{-3}). A PHIWC time series derived from GOES-14 1-min super rapid scan observations (Fig. 6)
210 shows that high IWC conditions (*in situ* total water content $> 0.5 \text{ gm}^{-3}$) can be resolved quite
211 well. The 3-dimensional ALPHA HIWC Potential product shows similar statistics when verified
212 against a reserved set of independent flight-level data from the three field campaigns (i.e., data
213 not used for training of the algorithm). For example, with an assumed HIWC Potential threshold
214 of 0.25 and an IWC threshold of 0.5 gm^{-3} , ALPHA POD is 76% and FAR is 25% in primarily

215 daytime conditions. Figure 7 shows the relationship between measured IWC and HIWC
216 Potential for 49 flights during three field campaigns as estimated by ALPHA. RDT has been
217 mainly compared with IWC measurements from the Robust Probe during the Cayenne field
218 campaign. When RDT cells are matched with IWC measurements, it appears that (for 11 out of
219 16 flights) 70% of values of IWC above 1.0 gm^{-3} fall within a RDT cell. For 4 flights, over 90% of
220 high IWC values fall within a RDT cell.

221 While the IWC threshold used to define high IWC is still under discussion by the research
222 community and aviation regulators, values of 0.5 g m^{-3} and 1.0 g m^{-3} have been used to compile
223 performance statistics. Currently, the *in situ* IWC threshold is the accepted metric within the ICI
224 community. However, the community accepts this in part only because of the lack of
225 comprehensive information about ICI events. *In situ* IWC exceeding the threshold value may be
226 only one of the criteria required for ICI events to occur. For example, there is some indication
227 that simply exceeding a particular IWC for a brief period of time may not be as hazardous to
228 engines as a longer duration exposure to moderate and high IWC. In addition, there are
229 differences in sensitivity of specific engines to high IWC exposure. Obtaining a better
230 understanding of these factors is critical for refining the existing products. Unfortunately, this
231 information is generally not provided by airlines and aircraft manufacturers to researchers, a
232 circumstance which limits further improvement of high IWC detection and nowcasting
233 techniques.

234 **OPERATIONAL APPLICATIONS**

235 In response to the ICI hazard, researchers have responded with a collection of prototype
236 methods for identifying high IWC conditions, and have verified the resulting products with

237 available research data. The products exhibit reasonable probabilities of detection, but often
238 with significant false alarm rates. Ongoing research will address the need for regional tuning of
239 algorithms, vertical variation of high IWC conditions, and short-term forecasting methods for
240 predicting the ICI hazard. In addition, the integration of geostationary satellite data from
241 multiple satellites (i.e., MSG, the GOES-R series, and Himawari-8) together with global NWP
242 models allows for the provision of operational ICI guidance products with global coverage.

243 In parallel with this research the International Civil Aviation Organization (ICAO) has
244 recognized a requirement by the international aviation industry for HIWC guidance products
245 and is working to develop service requirements. Outreach efforts are currently underway to
246 introduce high IWC detection capabilities to weather forecasters and airline users. Under a joint
247 effort by the Australian Bureau of Meteorology, NCAR, and the FAA, real-time ALPHA products
248 are being provided to industry users on a trial basis. The LaRC PHIWC products are being
249 provided to several NOAA national forecast centers and Central Weather Service Units to
250 enable near real-time identification of hazardous convection. RDT is now produced globally by
251 Météo-France using five geostationary satellites, and the product is available to aviation end-
252 users. Feedback from these users will be an important source of information for refining the
253 capability and utility of these products in real-world settings.

254 **RECOMMENDATIONS**

255 Working in the context of a larger international collaboration, the high IWC nowcasting
256 researchers have demonstrated the value of synergistic effort toward a common goal. As noted
257 by Pablo Perez Illana (HAIC project office, European Commission, Directorate-General for
258 Research & Innovation, Aviation), “the interdisciplinary, international and interactive approach

259 is worth highlighting". He notes that the HAIC-HIWC collaboration brings together experts from
260 numerous disciplines within the meteorology and aviation communities. It also serves as an
261 example for successful transatlantic and multilateral collaboration, being the largest European
262 Union co-funded aviation research project with North America.

263 The sustained collaborative effort between international teams devoted to the high IWC
264 nowcasting challenge has resulted in a set of prototype products for detecting ICI hazards.
265 Continued development and improvement of product performance depends on access by
266 researchers to detailed information on engine performance and meteorological conditions
267 during actual ICI events as well as additional *in situ* IWC measurements collected in future field
268 experiments. Feedback from users in operational settings is needed to define usage concepts
269 and methods for integrating high IWC products with other aviation weather products. Future
270 efforts will benefit from additional interaction with the aviation community to define product
271 performance requirements, determine how high IWC products can best support flight planning
272 and operations, and support the expected growing role of data analytics in aviation.

273 **ACKNOWLEDGEMENTS**

274 The authors thank the organizers, collaborators, and sponsors of the HAIC and HIWC
275 projects who enabled the collection of essential data sets for this work and provided support
276 for development of these products. The HAIC authors (De Laat, Defer, Delanoë, Grandin,
277 Moisselin, Parol) have received funding from the European Union's Seventh Framework
278 Program in research, technological development and demonstration under grant agreement
279 n°ACP2-GA-2012-314314. The research conducted by one of the authors (Haggerty) is in
280 response to requirements and funding by the Federal Aviation Administration (FAA). The views
281 expressed are those of the authors and do not necessarily represent the official policy or
282 position of the FAA. NCAR is sponsored by the National Science Foundation. NASA HIWC
283 research (Bedka) was supported by the Advanced Air Transport Technology Project within the
284 NASA Aeronautics Research Mission Directorate Advanced Air Vehicles Program.

285 **FOR FURTHER READING**

- 286 Ackerman, A. S., A. M. Fridlind, A. Grandin, F. Dezitter, M. Weber, J. W. Strapp, and A. V.
287 Korolev, 2015: High ice water content at low radar reflectivity near deep convection – Part
288 2: Evaluation of microphysical pathways in updraft parcel simulations. *Atmos. Chem. Phys.*,
289 15, 11729-11751, doi: 10.5194/acp-15-11729-2015.
- 290 Adams, E. 2018: The world's biggest jet engine is about to get a blast of ice. *Wired*, accessed 15
291 Jan 2018, <https://www.wired.com/story/testing-boeings-new-engine/>
- 292 Aviation Safety Network, 2016: FAA orders engine icing fixes for GENx-powered Boeing 787
293 Dreamliners. Flight Safety Foundation, accessed 1 Dec 2017, [http://news.aviation-](http://news.aviation-safety.net/2016/04/23/faa-orders-engine-icing-fixes-for-genx-powered-boeing-787-dreamliners/)
294 [safety.net/2016/04/23/faa-orders-engine-icing-fixes-for-genx-powered-boeing-787-](http://news.aviation-safety.net/2016/04/23/faa-orders-engine-icing-fixes-for-genx-powered-boeing-787-dreamliners/)
295 [dreamliners/](http://news.aviation-safety.net/2016/04/23/faa-orders-engine-icing-fixes-for-genx-powered-boeing-787-dreamliners/)
- 296 Bedka, K. M., and K. Khlopenkov, 2016: A probabilistic pattern recognition method for detection
297 of overshooting cloud tops using satellite imager data. *J. Appl. Meteor. Climatol.* **55**, 1983–
298 2005, [https://doi: 10.1175/JAMC-D-15-0249.1](https://doi.org/10.1175/JAMC-D-15-0249.1)
- 299 Bedka, K.M., J.T. Allen, H.J. Punge, M. Kunz, and D. Simanovic, 2018: A Long-Term Overshooting
300 Convective Cloud Top Detection Database Over Australia Derived From MTSAT Japanese
301 Advanced Meteorological Imager Observations. *J. Appl. Meteor. Climatol.*, **57**, 937-
302 951, <https://doi.org/10.1175/JAMC-D-17-0056.1>
- 303 Bravin, M., Strapp, J. W., and Mason, J., 2015: An investigation into location and convective
304 lifecycle trends in an ice crystal icing engine database, Tech. rep., SAE Technical Paper
305 2015-01-2130, SAE International, Warrendale, PA, doi:10.4271/2015-01-2130.

306 Ceccaldi M., Delanoë J., Hogan R. J., Pounder N. L., Protat A., Pelon J, 2013: From CloudSat-
307 CALIPSO to EarthCare: Evolution of the DARDAR cloud classification and its comparison to
308 airborne radar-lidar observations, *J. Geophys. Res., C: Oceans Atmos. ,* **118** (14), 7962-
309 7981.

310 Davison, C. R., Strapp, J. W., Lilie, L., Ratvasky, T. P., and Dumont, C., 2016: Isokinetic TWC
311 evaporator probe: Calculations and systemic error analysis, *8th Conference on Atmospheric*
312 *and Space Environments*, 17-21 June, Washington, DC, American Institute of Aeronautics
313 and Astronautics, <http://dx.doi.org/10.2514/6.2016-4060>

314 de Laat, A., Defer, E., Delanoë, J., Dezitter, F., Gounou, A., Grandin, A., Guignard, A., Meirink, J.
315 F., Moisselin, J.-M., and Parol, F., 2017: Analysis of geostationary satellite-derived cloud
316 parameters associated with environments with high ice water content, *Atmos. Meas. Tech.*,
317 **10**, 1359-1371, <https://doi.org/10.5194/amt-10-1359-2017>.

318 Delanoë, J., and R. J. Hogan, 2008: A variational scheme for retrieving ice cloud properties from
319 combined radar, lidar, and infrared radiometer, *J. Geophys. Res.*, **113**, D07204,
320 doi:10.1029/2007JD009000.

321 Dezitter, F., Grandin, A., Brenguier, J.-L., Hervy, F., Schlager, H., Villedieu, P., and Zalamansky, G.: HAIC –
322 High Altitude Ice Crystals, 5th AIAA Atmospheric and Space Environments Conference, American
323 Institute of Aeronautics and Astronautics, available at: [http://arc.aiaa.org/doi/abs/10.2514/6.](http://arc.aiaa.org/doi/abs/10.2514/6.2013-2674)
324 2013-2674 (last access: 9 February 2015), 2013.

325 Grandin, A., J.-M. Merle, M. Weber, J. Strapp, A. Protat, and P. King, 2014: AIRBUS Flight Tests
326 in High Total Water Content Regions, *6th Conference on Atmospheric and Space*
327 *Environments*, 16-19 June, Atlanta, GA, American Institute of Aeronautics and Astronautics,
328 <http://arc.aiaa.org/doi/abs/10.2514/6.2014-2753>

329 Grzych, M., and J. Mason, 2010: Weather conditions associated with jet engine power loss and
330 damage due to ingestion of ice particles: What we've learned through 2009. 14th Conf. on
331 Aviation, Range and Aerospace Meteorology, Atlanta, GA, Amer. Meteor. Soc., 6.8.
332 [Available online at <https://ams.confex.com/ams/pdfpapers/165923.pdf>.]

333 Grzych, M., Tritz, T., Mason, J., Bravin, M. et al., 2015: Studies of cloud characteristics related to
334 jet engine ice crystal icing utilizing infrared satellite imagery, SAE Technical Paper 2015-01-
335 2086, SAE International, Warrendale, PA, doi:10.4271/2015-01-2086.

336 Haggerty, J., F. McDonough, J. Black, G. Cuning, G. McCabe, M. Politovich, C. Wolff, 2012: A
337 system for nowcasting atmospheric conditions associated with jet engine power loss and
338 damage due to ingestion of ice particles, 2012: *4th Conference on Atmosphere and Space
339 Environment Conference*, New Orleans, LA, American Institute of Aeronautics and
340 Astronautics, 25-28 June, AIAA-2012-3234.

341 Lawson, R.P., L. J. Angus, and A.J. Heymsfield. 1998: Cloud particle measurements in
342 thunderstorm anvils and possible weather threat to aviation, *Journal of Aircraft*, **35**, 113-
343 121.

344 Leroy, D., E. Fontaine, A. Schwarzenboeck, J. W. Strapp, A. Korolev, G. McFarquhar, R. Dupuy, C.
345 Gourbeyre, L. Lilie, A. Protat, J. Delanoë, F. Dezitter, and A. Grandin, 2017: Ice Crystal Sizes
346 in High Ice Water Content Clouds. Part II: Statistics of Mass Diameter Percentiles in Tropical
347 Convection Observed during the HAIC/HIWC Project. *J. Atmos. Oceanic Technol.*, **34**, 117-
348 136, doi:10.1175/JTECH-D-15-0246.1.

349 Mason, J.G., J.W. Strapp, and P. Chow, 2006: The ice particle threat to engines in flight, *44th*
350 *Aerospace Sciences Meeting*, Reno, NV, American Institute of Aeronautics and Astronautics,
351 9-12 January, AIAA-2006-206.

352 Protat A., Delanoë, J., Bouniol, D., et al., 2007: Evaluation of ice water content retrievals from
353 cloud radar reflectivity and temperature using a large airborne in-situ microphysical
354 database, *J. Appl. Meteorol.*, **46**, 557–572.

355 Rugg, A., J. Haggerty, G. McCabe, R. Palikondra, and R. Potts, High ice water content conditions
356 around Darwin: Frequency of occurrence and duration as estimated by a nowcasting
357 model," *9th Conference on Atmosphere and Space Environment* Denver, USA, 5-9 Jun 2017,
358 American Institute of Aeronautics and Astronautics ,
359 <https://arc.aiaa.org/doi/abs/10.2514/6.2017-4472>

360 Stanford, M. W., Varble, A., Zipser, E., Strapp, J. W., Leroy, D., Schwarzenboeck, A., Potts, R.,
361 and Protat, A., 2017: A ubiquitous ice size bias in simulations of tropical deep convection,
362 *Atmos. Chem. Phys.*, **17**, 9599-9621, <https://doi.org/10.5194/acp-17-9599-2017>.

363 Strapp, J. W., and Coauthors, 2016: The High Ice Water Content (HIWC) study of deep
364 convective clouds: Report on science and technical plan, FAA Rep. DOT/FAA/TC-14/31, 105
365 pp. [Available online at www.tc.faa.gov/its/worldpac/techrpt/tc14-31.pdf.]

366 Yost, C. R., Bedka, K. M., Minnis, P., Nguyen, L., Strapp, J. W., Palikonda, R., Khlopenkov, K.,
367 Spangenberg, D., Smith Jr., W. L., Protat, A., and Delanoë, J., 2018: A prototype method for
368 diagnosing high ice water content probability using satellite imager data, *Atmos. Meas.*
369 *Tech.*, **11**, 1615-1637, <https://doi.org/10.5194/amt-11-1615-2018>

370 **Tables**

371 Table 1: HIWC Diagnostic Products

Product Name (developer)	Input Data Type(s)	Output Field
MSG-CPP HIWC Mask (KNMI)	CPP Satellite Products	Yes/No HIWC
DARDAR (CNRS)	CloudSat, CALIPSO	IWC Vertical Profiles
PHIWC (NASA)	Overshooting Cloud Top / Anvil Texture Detection, LaRC SatCORPS, GEO Cloud Property Retrieval	HIWC Potential
ALPHA (NCAR)	NWP Model, Groundbased Radar, GEO satellite products	HIWC Potential
RDT (Météo-France)	GEO satellite data (main input data), NWP, Lightning	Areas of rapidly developing convection

372

373

374

375 Table 2: HIWC Satellite and Nowcasting Workshops hosted by the HAIC-HIWC partners

Location	Date
Toulouse, France	Oct 2015
Melbourne, Australia	Nov 2015
Toronto, Canada	May 2016
Toulouse, France	Sept 2016
Capua, Italy	Dec 2016
Toulouse, France	Nov 2017

376

377 **Figure Captions**

378 Figure 1: Locations of confirmed Ice Crystal Icing Events on Boeing aircraft as of 2015. Adapted
379 from M. Bravin, The Boeing Corp.

380
381 Figure 2: (a) Tropopause-relative GOES-14 IR brightness temperature (GOES minus tropopause).
382 Cool colors indicate cloud tops near to or above the tropopause. (b) GOES IR overshooting top
383 detection probability (color shading, values > 0.7 shown) and visible texture detection (magenta
384 contours). (c) NASA LaRC Probability of High Ice Water Content (PHIWC) overlaid with a 10-
385 minute segment of IKP2 total water content (TWC) collected by the NASA DC-8 aircraft during
386 the 2015 Ft. Lauderdale flight campaign. Aircraft positions are colored by the observed TWC,
387 showing a sharp transition when the aircraft entered a region of high PHIWC (> 0.6) driven by
388 cloud tops near the tropopause and close proximity to overshooting cloud tops (right).

389
390 Figure 3: NCAR's ALPHA HIWC Potential product (gray scale indicates maximum value in vertical
391 column) in the Gulf of Mexico on 16 August 2015 at 1745 UTC. The black contour encloses an
392 area with HIWC Potential > 0.2 . Color scale indicates ice water content along a 30-minute flight
393 segment of the NASA DC-8.

394
395 Figure 4: Operating area of the HAIC-HIWC Darwin flight campaign (yellow polygon) with
396 groundbased radar coverage indicated by gray rings, including the research CPOL radar (blue
397 ring) (top). The red ring shows a 300 nmi distance reference. The SAFIRE Falcon 20 aircraft

398 prepares for a research flight (middle). Monsoon convection sampled within the Darwin
399 operating area (bottom). Photos provided by T. Ratvasky.

400

401 Figure 5: Percentage (probability of detection) of MSG-CPP pixels identified by the High IWC
402 mask as a function of the maximum IWC values in DARDAR IWC profiles. DARDAR (raDAR/liDAR)
403 combines data from two earth observation satellites (CALIPSO lidar and CloudSat radar; see de
404 Laa (2017) for details) and provides high vertical resolution cloud and aerosol profiles,
405 including cloud ice/water content The colored lines indicate the percentage of MSG-CPP pixels
406 that qualify for the High IWC mask pixels for DARDAR profiles with the height of the maximum
407 IWC above the given altitude. The black dots indicate the number of MSG-CPP cloudy pixels
408 identified as ice as a function of the maximum IWC values in DARDAR IWC profiles. Figure
409 adapted from deLaat et al. (2017).

410

411 Figure 6: (top) In-situ total water content (TWC) observations from the IKP2 sensor collected on
412 16 August 2015 aboard the NASA DC-8 aircraft during the Ft. Lauderdale flight campaign. IKP-2
413 TWC is averaged to 5-sec (grey) and 45-second (black) intervals. The 45-sec time window, when
414 coupled with the DC-8 airspeed, better represents the area of a GOES satellite infrared channel
415 pixel (top panel). The LaRC Probability of High Ice Water Content (PHIWC) product based on
416 inputs with (black) and without (grey) datasets derived using GOES visible channel information
417 (bottom panel).

418

419 Figure 7: Box plot showing relationship between measured TWC and HIWC Potential estimated
420 by NCAR's ALPHA which was objectively trained using airborne *in situ* data from the Isokinetic
421 Probe for three field experiments as described in the text. The median (50th percentile) is
422 indicated in red, the blue box extends from the 25th to 75th percentile, and the dashed lines
423 extend to the minimum/maximum non-outlier values.

424

425 **Figures**

426

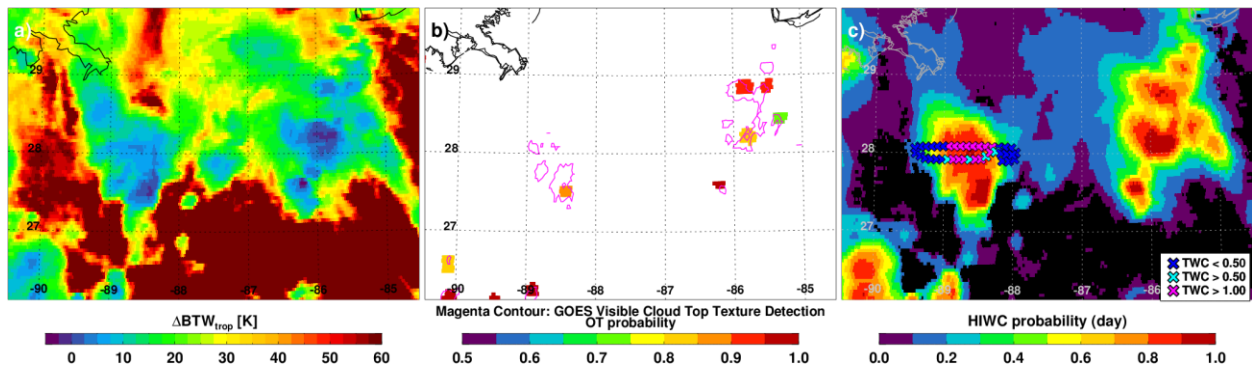


427

428 Figure 1: Locations of confirmed Ice Crystal Icing Events on Boeing aircraft as of 2015. Adapted
429 from M. Bravin, The Boeing Corp.

430

431



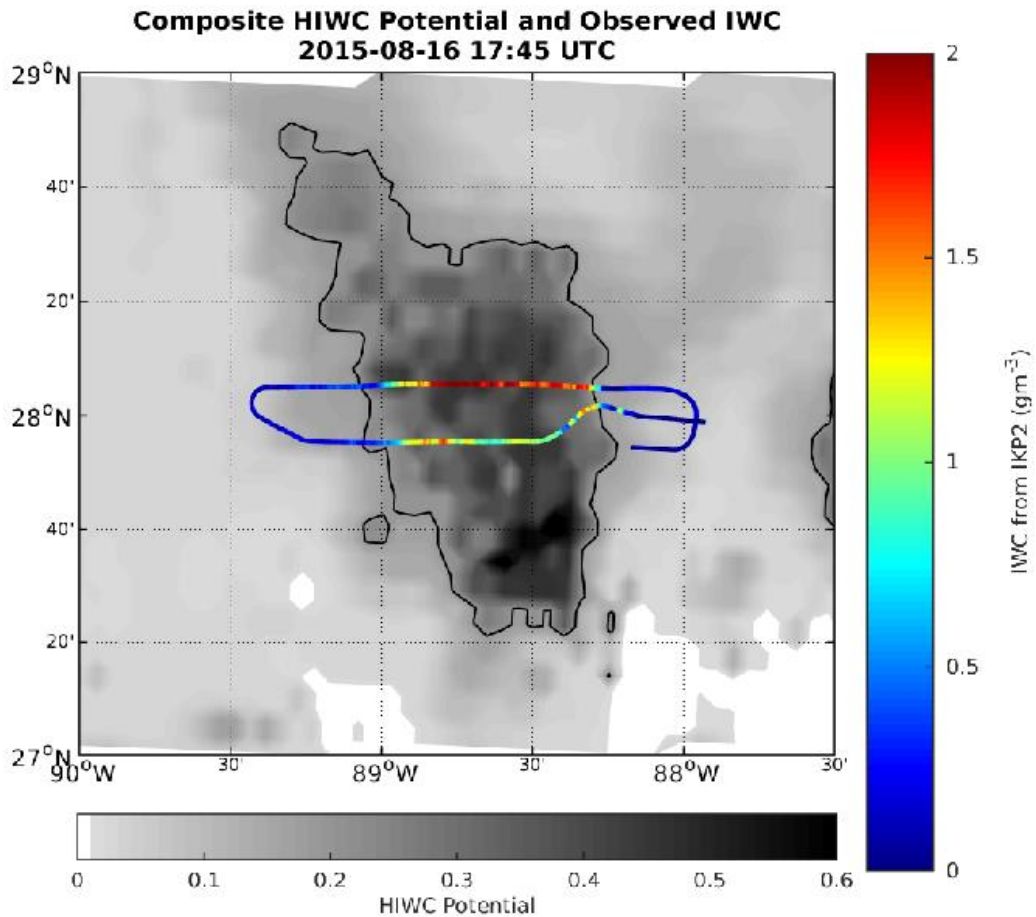
432

433

434 Figure 2: (a) Tropopause-relative GOES-14 IR brightness temperature (GOES minus tropopause).
435 Cool colors indicate cloud tops near to or above the tropopause. (b) GOES IR overshooting top
436 detection probability (color shading, values > 0.7 shown) and visible texture detection (magenta
437 contours). (c) NASA LaRC Probability of High Ice Water Content (PHIWC) overlaid with a 10-
438 minute segment of IKP2 total water content (TWC) collected by the NASA DC-8 aircraft during
439 the 2015 Ft. Lauderdale flight campaign. Aircraft positions are colored by the observed TWC,

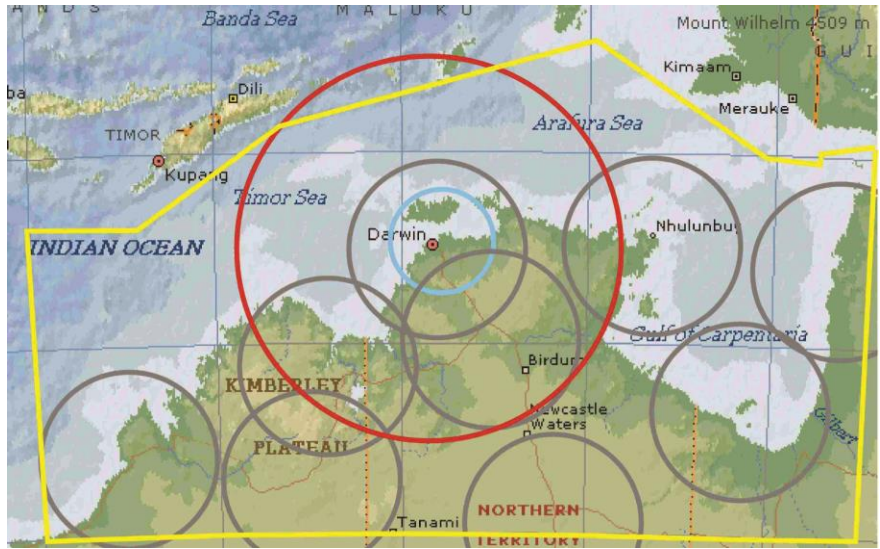
440 showing a sharp transition when the aircraft entered a region of high PHIWC (> 0.6) driven by
441 cloud tops near the tropopause and close proximity to overshooting cloud tops (right).

442
443
444
445
446



447
448

449 Figure 3: NCAR's ALPHA HIWC Potential product (gray scale indicates maximum value in vertical
450 column) in the Gulf of Mexico on 16 August 2015 at 1745 UTC. The black contour encloses an
451 area with HIWC Potential > 0.2. Color scale indicates ice water content along a 30-minute
452 segment of the NASA DC-8 flight shown in Fig. 2.



453

454

455

456

457

458

459

460



461

462

463

464

465

466

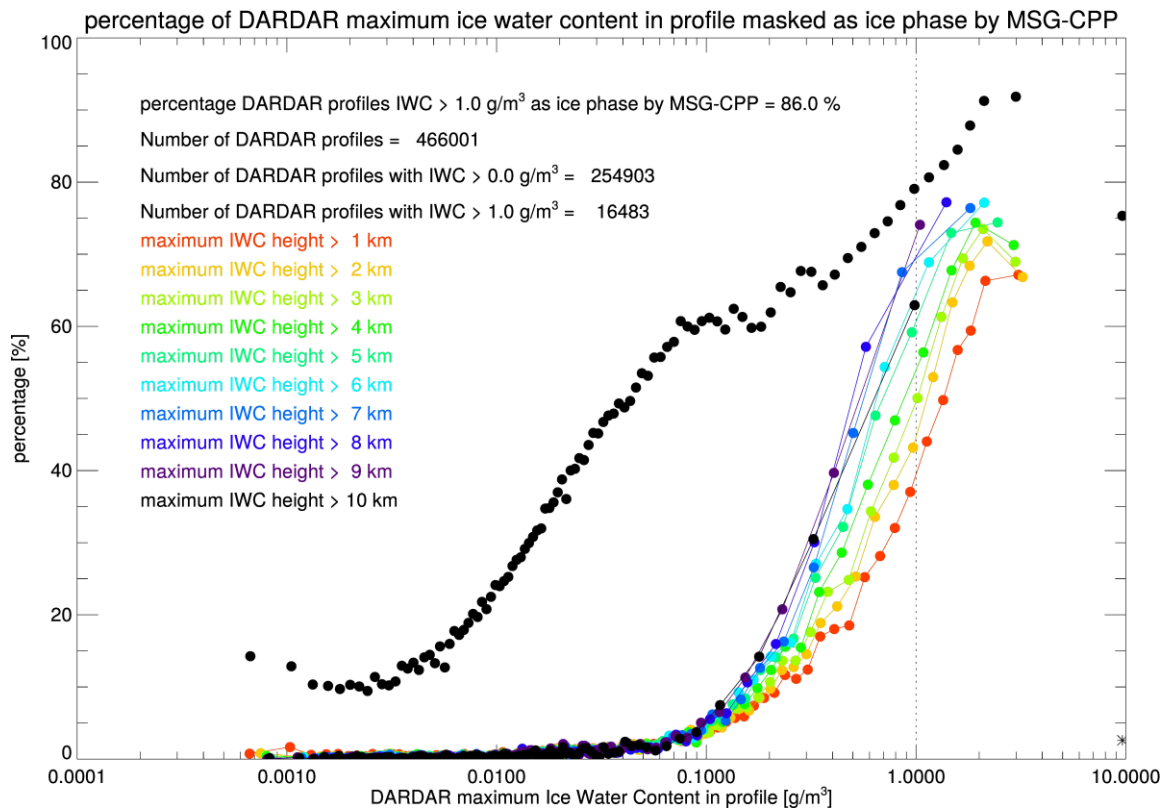
467

468



469 Figure 4: Operating area of the HAIC-HIWC Darwin flight campaign (yellow polygon) with
 470 groundbased radar coverage indicated by gray rings, including the research CPOL radar (blue
 471 ring) (top). The red ring shows a 300 nmi distance reference. The SAFIRE Falcon 20 aircraft
 472 prepares for a research flight (middle). Monsoon convection sampled within the Darwin
 473 operating area (bottom). Photos provided by T. Ratvasky.

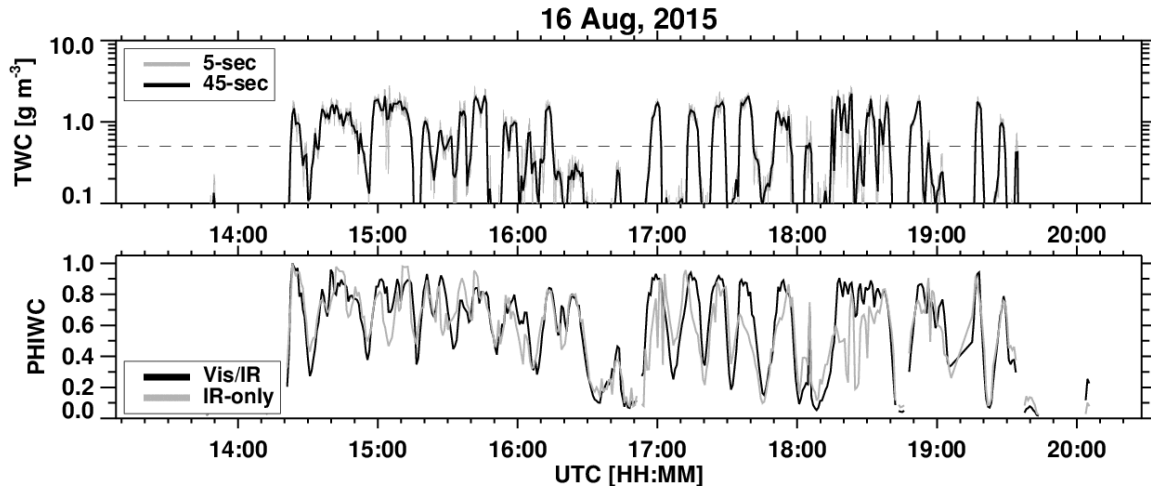
474
475
476
477



478
479

480 Figure 5: Percentage (probability of detection) of MSG-CPP pixels identified by the High IWC
481 mask as a function of the maximum IWC values in DARDAR IWC profiles. DARDAR (raDAR/liDAR)
482 combines data from two earth observation satellites (CALIPSO lidar and CloudSat radar; see de
483 Laa et al. (2017) for details) and provides high vertical resolution cloud and aerosol profiles,
484 including cloud ice/water content The colored lines indicate the percentage of MSG-CPP pixels
485 that qualify for the High IWC mask pixels for DARDAR profiles with the height of the maximum
486 IWC above the given altitude. The black dots indicate the number of MSG-CPP cloudy pixels
487 identified as ice as a function of the maximum IWC values in DARDAR IWC profiles. Figure
488 adapted from deLaat et al. (2017).

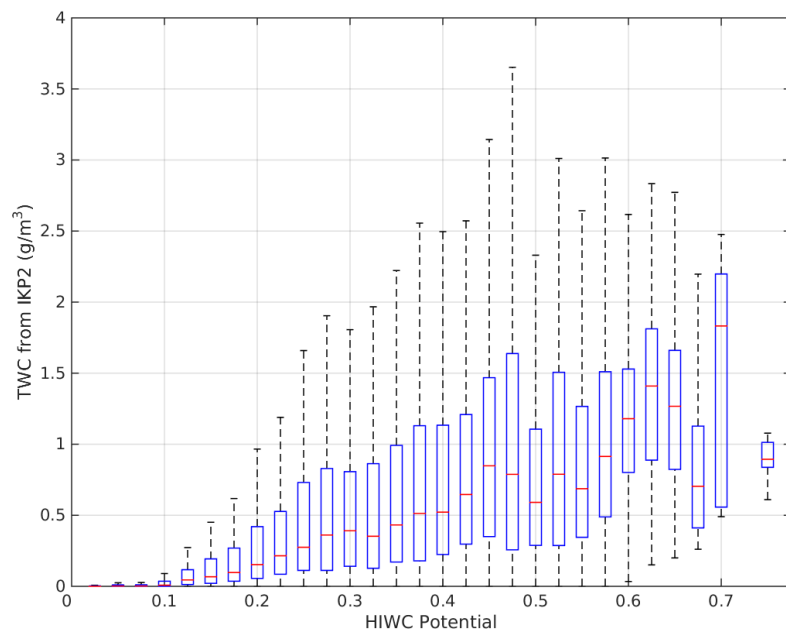
489



490

491 Figure 6: In-situ total water content (TWC) observations from the IKP2 sensor collected on 16
 492 August 2015 aboard the NASA DC-8 aircraft during the Ft. Lauderdale flight campaign. IKP-2
 493 TWC is averaged to 5-sec (grey) and 45-second (black) intervals. The 45-sec time window, when
 494 coupled with the DC-8 airspeed, better represents the area of a GOES satellite infrared channel
 495 pixel (top panel). The LaRC Probability of High Ice Water Content (PHIWC) product based on
 496 inputs with (black) and without (grey) datasets derived using GOES visible channel information
 497 (bottom panel).

498



500

501 Figure 7: Box plot showing relationship between measured TWC and HIWC Potential estimated
 502 by NCAR's ALPHA which was objectively trained using airborne *in situ* data from the Isokinetic
 503 Probe for three field experiments as described in the text. The median (50th percentile) is
 504 indicated in red, the blue box extends from the 25th to 75th percentile, and the dashed lines
 505 extend to the minimum/maximum non-outlier values.

